Available online at www.sciencedirect.com
SCIENCE DIRECT®
Surface Science 572 (2004) 146–161
SURFACE SCIENCE
www.elsevier.com/locate/susc

# Fundamental studies of titanium oxide-Pt(100) interfaces II. Influence of oxidation and reduction reactions on the surface structure of $TiO_x$ films on Pt(100)

Taketoshi Matsumoto [1], Matthias Batzill [2], Shuchen Hsieh [3], Bruce E. Koel *

*Department of Chemistry, University of Southern California, Los Angeles, CA 90089-0482, USA*

Received 6 February 2004; accepted for publication 7 August 2004
Available online 26 August 2004

**Abstract**

Chemical reactions of titanium-oxide ultrathin films on Pt(100) and associated changes in the surface structure have been studied by STM (scanning tunneling microscopy), LEED (low energy electron diffraction), AES (Auger electron spectroscopy) and TPD (temperature programmed desorption). Such reactions and changes have important consequences for understanding and modeling of catalysis of related systems and the oxide structures formed have an additional significance in their subsequent use as masks or templates on Pt(100) in studies relevant to nanotechnology. In a previous paper [Matsumoto et al., Surf. Sci., submitted] we characterized a monolayer-oxide film exhibiting a $(3\times5)$ structure on Pt(100) as due to $Ti_2O_3$. Herein, we characterize changes that occur in this film during subsequent oxidation and reduction reactions, and propose models for the structures of $TiO_x$ films that are formed. $O_3$ (ozone) or $NO_2$ (nitrogen dioxide) oxidation of the $(3\times5)$-$Ti_2O_3$ film at 600 K and subsequent annealing to 700–950 K in vacuum produced disordered oxide regions and domains of a $(4\times13)$ structure that we attribute to a $TiO_2$ film with a square –Ti–O– net. This film is transformed further after annealing at 1000–1100 K to $(3\times5)$-$Ti_2O_3$ domains and domains exhibiting a $(2\sqrt{2}\times2\sqrt{2})R45°$ structure that we attribute to a $Ti_5O_8$ film. Additional heating of this film to 1200 K forms primarily a $(3\times5)$-$Ti_2O_3$ oxide film. Three dimensional clusters of $TiO_2$ are also produced by these oxidation and annealing procedures. Initial oxidation of a "flat" $(3\times5)$ oxide film at 600 K reconstructs this surface to form a *multilayer*, *porous oxide film*, and more extensive oxidation eventually forms a much less porous oxide film with *pyramidal oxide crystallites*. Oxidation of the $(3\times5)$ structure using NO (nitric oxide) differs from that above in that the $(4\times13)$ structure was not observed, but oxidation does produce the $(2\sqrt{2}\times2\sqrt{2})R45°$ structure due to dissociation of NO at Pt sites. The titanium oxide films on Pt(100) described above block adsorption of CO at Pt sites at temperatures above 210 K, and also these surfaces do not oxidize CO. Exposure to a stronger reducing agent, HCOOH (formic

* Corresponding author. Tel.: +1 213 740 4126; fax: +1 213 740 3972.
*E-mail address:* koel@usc.edu (B.E. Koel).
[1] Present address: Laboratory for Entrepreneurship, University of Tsukuba, Ibaraki 305-8573, Japan.
[2] Present address: Department of Physics, Tulane University, New Orleans, LA 70118.
[3] Present address: NIST, Gaithersburg, MD 20899.

0039-6028/$ - see front matter 
doi:10.1016/j.susc.2004.08.005

acid), leads to molecular formic acid desorption at 371 K from a thick titanium oxide film containing $(3\times5)$ domains without a trace of surface reduction. However, formic acid exposures at low temperatures followed by heating in TPD reduce the $(4\times13)$ oxide structure, which is inert to reduction by CO, to form $(3\times5)$ and $(2\sqrt{2}\times2\sqrt{2})R45°$ domains. Formic acid is also desorbed molecularly from clean Pt(1 0 0) at 330 K.


*Keywords:* Low electron energy diffraction (LEED); Scanning tunneling microscopy; Oxidation; Surface chemical reaction; Platinum; Titanium oxide

## 1. Introduction

Many ordered structures of oxide thin films have been produced on metal single crystal surfaces in order to study oxide-surface properties and epitaxial growth mechanisms of oxides. Understanding the structural and mechanical nature, along with the electronic and chemical properties, of oxide films is important for a wide range of applications, including those in electronic devices and recording media [1], sensors, and heterogeneous catalysts. In particular, the migration of oxide films onto metal particles present in supported metal catalysts has been reported for catalysts showing SMSI (strong metal-support interaction). Also, thin oxide films formed on metal substrates have been used as model surfaces to observe phenomena at the atomic level, including bifunctional catalysis [2], special properties of oxide-metal boundaries [2,3], and alloy formation [4]. These films have an advantage in fundamental studies that electron- and ion-based spectroscopic methods, and STM (scanning tunneling microscopy), can be utilized because of their higher conductivity compared to bulk oxides. Also, the higher thermal conductivity of these samples allows for the use of simple heating systems [5].

Self-assembled oxide thin films provide exquisite capability for modifying surfaces at the nanoscale or atomic level. Ultrathin films can be used to "hide" the substrate partially [6] in order to limit interactions between adsorbates and the substrate. Another exciting application is to use such films as a "surface mesh", net, or structured template for subsequent deposition. For example, the oxide template could be used to support metal clusters possessing a small size distribution that could be produced by subsequent evaporation of an immiscible metal followed by slight annealing to drive clustering. Such an approach should be helpful for studying quantum size effects in metal cluster catalysts and the dramatic activity changes that have been reported to depend on the metal cluster size [7].

Chemical properties of titanium oxide thin films are of particular interest. It has been reported for catalysts exhibiting SMSI that $TiO_x$ ($x\sim1$) films encapsulate Pt clusters on the $TiO_2$ support and block adsorption sites of CO and $H_2$ [11]. However, few reactions have been studied on model systems composed of $TiO_x$ thin films on Pt single crystal surfaces. Adsorption and chemical reactions have been studied on $TiO_2$(1 1 0) single crystal surfaces rather extensively. Decomposition of HCOOH (formic acid) [12] and dissociative adsorption of $CH_3OH$ (methanol) [13] were reported on $TiO_2$(1 1 0) terraces. On defect sites with bridging O vacancies, stronger adsorption of CO [14], dissociative adsorption of $H_2$ [15,16] and $H_2O$ [17,18], and decomposition of NO [19] were found, in addition to oxidation with $O_2$ [20]. These results suggest that the terraces, and especially the perimeters, of titanium oxide films could play important roles in surface reactions.

In a previous paper, we produced a titanium-oxide monolayer film exhibiting a $(3\times5)$ structure by Ti evaporation in an $O_2$ background on a Pt(1 0 0) substrate and then annealing in $O_2$ [8]. This structure was attributed to $Ti_2O_3$. This is different from the $TiO_2$ thin film with a structure similar to $TiO_2$(1 1 0) [10] that was produced on Pt(1 1 1) by using a similar procedure [9], and this illustrates the importance of the substrate structure and chemistry. At the outset of these investigations, we proposed that new, ordered, $TiO_2$ thin films could be produced on Pt(1 0 0) by varying the deposition and growth conditions, and in

particular by using oxidants stronger than $O_2$, such as $O_3$ (ozone) and $NO_2$ (nitrogen dioxide), or perhaps NO (nitric oxide). We report here on our investigations of the structure and chemical properties of deeply oxidized titanium films on Pt(1 0 0) as characterized by STM, LEED (low electron energy microscopy), AES (Auger electron spectroscopy) and TPD (temperature programmed desorption). While theoretical calculations are critically needed to properly elucidate these oxide structures, tentative "net-like" models for two new, ordered, titanium-oxide film structures on Pt(1 0 0) are proposed in hopes of stimulating such calculations and further experiments.

## 2. Experimental methods

Experiments were carried out in a UHV (ultra-high vacuum) chamber with capabilities for STM, LEED, TPD, and AES [21]. Preparation of a clean Pt(1 0 0) surface and the method of Ti evaporation are described elsewhere [8]. The procedure to prepare high purity ozone is also described in a previous report [22].

$CH_3OH$ (methanol) and HCOOH (formic acid) were used after several freeze-pump-thaw cycles and checks of the purity using the mass spectrometer in the UHV chamber. Peak-to-peak height ratios in AES were obtained using the Pt (237 eV), Ti (387 eV), O (510 eV) and C (272 eV) signals. Sensitivities for those transitions are 1:2:2.4:1, respectively [23]. All STM images were acquired in constant-current mode with the sample at 300 K.

The coverage where one layer of a film attributed to $Ti_2O_3$ covered the Pt(1 0 0) surface, as determined by STM, and also where $TiO_2$ assigned to a second layer started to appear in XPS [8] was defined to be 1 ML (monolayer).

## 3. Results

### 3.1. Oxidation of a titanium oxide film on Pt(1 0 0) by using $NO_2$ or $O_3$

A titanium-oxide monolayer film exhibiting a $(3\times5)$ structure, attributed to $Ti_2O_3$, can be produced by Ti evaporation in an $O_2$ background on Pt(1 0 0) and annealing in $O_2$ [8]. We attempted to carry out a deeper oxidation of this oxide film on Pt(1 0 0) by using stronger oxidants, $NO_2$ and $O_3$. $NO_2$ or $O_3$ exposures of 1–100 L on the $(3\times5)$ oxide film at a coverage above 1 ML at 200 K were carried out. TPD spectra following these exposures showed no clear desorption product peaks in signals monitored at 14 (N), 16 (O), 28 ($N_2$ and CO), 30 (NO), 32 ($O_2$), 44 ($N_2O$), and 46 ($NO_2$) amu. However, after heating to 600–1000 K during TPD, an additional LEED pattern was observed. Yet another, different structure could be obtained by deeper oxidation using 1–100-L $NO_2$ or $O_3$ exposures on the $(3\times5)$ oxide film on Pt(1 0 0) at 600 K and subsequently annealing to even higher temperatures in vacuum. Both of these new structures are described below.

#### 3.1.1. Formation of a titanium oxide film on Pt(1 0 0) with a $(4\times13)$ structure

Oxidation of a $(3\times5)$ oxide film [8] by exposures of $NO_2$ or $O_3$ on the surface at 600 K and subsequent annealing at 700–950 K produced a new, ordered structure in LEED. The observed LEED pattern, along with a simple simulation of the LEED pattern corresponding to a $(4\times13)$ structure, are shown in Fig. 1(a) and (b), respectively. The ellipses in the two figures encircle corresponding spots. Only some of the simulated LEED spots were observed in the measured LEED pattern because of dynamical effects and small domain sizes. This structural change was associated with a change in the Pt:Ti:O AES ratio from 1:3:3.5 to 1:3:4. XPS studies reported elsewhere [8] were used to attribute the $(4\times13)$ structure to a $TiO_2$ film.

Fig. 2(a) is an STM image of the $(4\times13)$ oxide film. Five different types of domains labeled as *A* and *G–J* were observed. *G* domains have a row structure with a periodicity that is 13 times larger than the width of a $(1\times1)$-Pt(1 0 0) unit cell. We assign these domains to the $(4\times13)$ oxide structure. *H* domains are due to an oxide film with a $(2\sqrt{2}\times2\sqrt{2})R45°$ structure (as discussed in detail below), and *I* domains are due to a disordered oxide film. *J* domains are due to one layer of Pt clusters with a height of 0.2 nm, and *A* domains

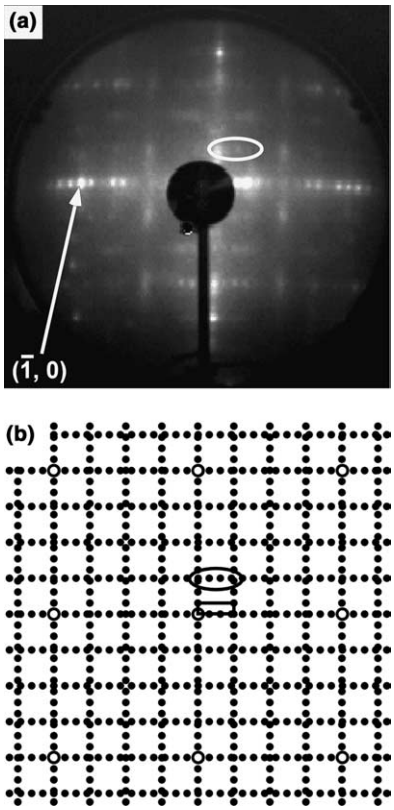


Fig. 1. (a) LEED pattern of the $(4\times13)$ structure produced by 6-L $NO_2$ oxidation of the $(3\times5)$ oxide film on Pt(100) at 600 K and annealing at 950 K in vacuum. (b) Simulated LEED pattern for a $(4\times13)$ unit cell. The rectangle given in (b) indicates the unit cell, and the superimposed ellipses in each figure encircle corresponding spots. The open circles indicate the primary beams for the $(1\times1)$-Pt(100) surface.

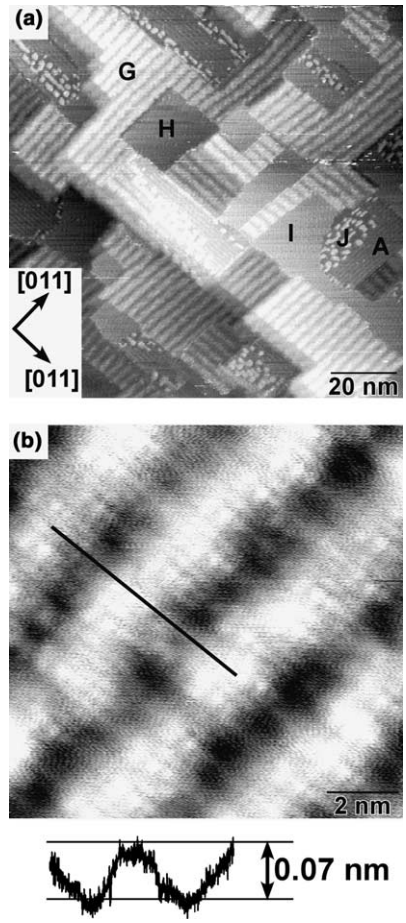


Fig. 2. STM topographs from a titanium-oxide film on Pt(100) exhibiting a $(4\times13)$ structure. (a) Surface region manifesting the $(4\times13)$ structure ($V_s = 0.11$V, $I_t = 1.85$ nA). Domains labeled *A*, *G*, *H*, *I* and *J* are assigned respectively to bare $(5\times20)$-Pt(100), $(4\times13)$ oxide structure, $(2\sqrt{2}\times2\sqrt{2})R45°$ oxide structure (seen more clearly in Fig. 4), disordered oxide domains and Pt clusters. (b) High-resolution image ($V_s = -0.54$ V, $I_t = 1.5$ nA) showing the Moiré pattern from the $(4\times13)$ oxide structure. The cross-section of the line scan indicated in the bottom image is shown directly below the image.

are due to $(5\times20)$-Pt(100) patches on the substrate. The structure of the *A* domains was confirmed by expanded images obtained for these domains (not shown). Fig. 2(b) shows an expanded image from a *G* domain, which additionally reveals that the Moiré pattern contains ordered, bright spots. The line scan indicated in this STM image gives a cross-section that is displayed below the image, and this shows an apparent corrugation of 0.07 nm for the Moiré structure.

Repeating the $NO_2$ or $O_3$ oxidation of these films at 600 K and annealing at 700–900 K increased the area of domains labeled as *I* and *J*, and also caused the appearance of $TiO_2$ clusters as identified elsewhere [8].

### *3.1.2. Formation of a titanium oxide film on Pt(100) with a $(2\sqrt{2}\times2\sqrt{2})R45°$ structure*

A $(2\sqrt{2}\times2\sqrt{2})R45°$ structure was obtained by annealing the $(4\times13)$ surface to 1000–1100 K in vacuum. This structure was observed locally after the $(3\times5)$ surface was exposed to $NO_2$ or $O_3$ with the sample below 300 K and then annealed at 800–1100 K.

The observed LEED pattern from the $(2\sqrt{2}\times 2\sqrt{2})R45°$ structure is shown in Fig. 3(a) and the corresponding simulation is shown in Fig. 3(b). The STM topogragh in Fig. 4(a) revealed that the $(2\sqrt{2}\times 2\sqrt{2})R45°$ film is built with a square net or "surface mesh". An expanded view of this structure is shown in Fig. 4(b). The brightest and darkest dots were observed at the corners and center of the unit cell, respectively. A cross-section along the straight line superimposed on the image is shown directly below and indicates that the corrugation of this structure is 0.07 nm.

Three types of defects, denoted as $H1$–$H3$ in Fig. 5, were found in $(2\sqrt{2}\times 2\sqrt{2})R45°$ domains

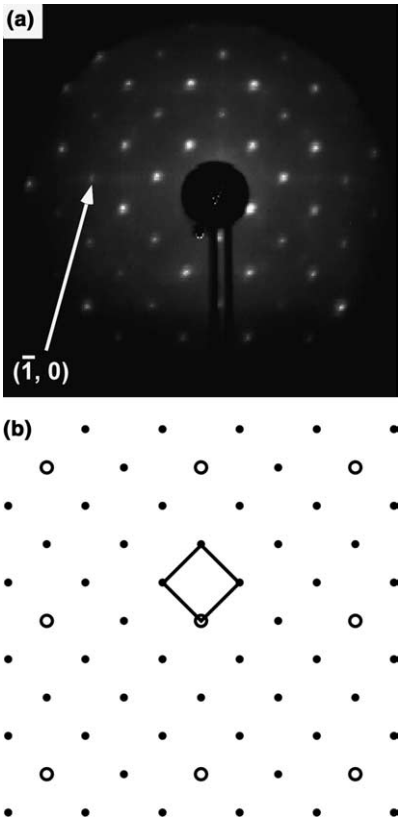


Fig. 3. (a) LEED pattern of the $(2\sqrt{2}\times 2\sqrt{2})R45°$ structure produced by annealing a $(4\times 13)$ oxide structure at 1000 K in vacuum. (b) Simulated LEED pattern for a $(2\sqrt{2}\times 2\sqrt{2})R45°$ unit cell. The rectangle given in (b) indicates the unit cell, and the open circles indicate the primary beams for the $(1\times 1)$-Pt(100) surface.

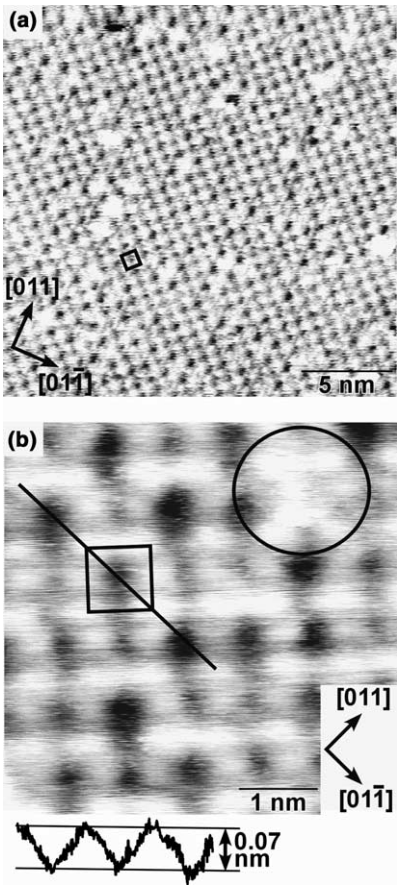


Fig. 4. STM topographs from a titanium-oxide film on Pt(100) exhibiting a $(2\sqrt{2}\times 2\sqrt{2})R45°$ structure. (a) Surface region manifesting an ordered domain ($V_s = 0.11$ V, $I_t = 1.85$ nA). (b) High-resolution image ($V_s = 0.14$ V, $I_t = 0.84$ nA). A defect (denoted as $H1$ in Fig. 5) is highlighted with a circle. The cross-section of the line scan indicated in the bottom image is shown directly below the image. Superimposed squares indicate the $(2\sqrt{2}\times 2\sqrt{2})R45°$ unit cell.

at a concentration of 10–15%. The apparent height of these defects, $H1$–$H3$, from bright corners of the net are $0.10\pm 0.02$ nm, $0.00\pm 0.01$ nm, $-0.07\pm 0.01$ nm, respectively.

A submonolayer coverage of the $(2\sqrt{2}\times 2\sqrt{2})R45°$ structure could be reduced to the $(3\times 5)$ structure by annealing at 1200 K in vacuum. This surface could be reoxidized by $O_3$ or $NO_2$ to form the $(4\times 13)$ structure, but this reoxidation was accompanied by the formation of $TiO_2$ clusters and bare Pt domains.

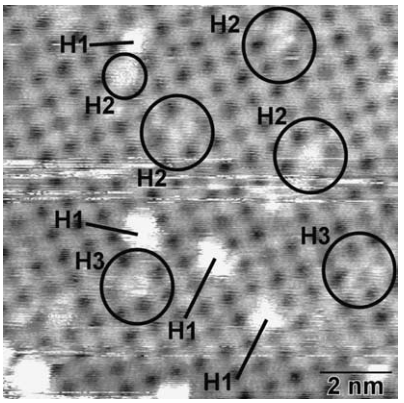


Fig. 5. STM topograph showing defect sites on a titanium-oxide film on Pt(100) exhibiting a $(2\sqrt{2}\times 2\sqrt{2})R45°$ structure ($V_s = 0.39$ V, $I_t = 0.87$ nA). We attribute the defects labeled $H1$–3 as due to population of a second layer, Ti atoms in the center of the unit cell, and rotated $(2\sqrt{2}\times 2\sqrt{2})R45°$ nets, respectively.

### 3.1.3. Deep oxidation of a titanium oxide film on Pt(100) with a (3 × 5) structure

Deep oxidation of the $(3\times 5)$-$Ti_2O_3$ film on Pt(100) carried out with $NO_2$ and $O_3$ was observed by using STM to reveal the mechanism of $TiO_2$ cluster formation. Fig. 6(a) shows an STM image after oxidation using 3-L $O_3$ with the substrate at 300 K carried out on the homogeneous $(3\times 5)$ surface (as seen in Fig. 4 of Part I [8]). Oxidation started mainly from step edges as highlighted by the superimposed black ellipse. The magnified view shown in Fig. 6(b) revealed row structures that are similar to those in the $(4\times 13)$ structure. About 90% of the area was recovered as the homogeneous $(3\times 5)$ surface after annealing to 900 K. However, this was accompanied by formation of $(5\times 20)$-Pt(100) domains and $TiO_2$ islands.

After dosing 3-L $O_3$ on the surface at 600 K, Fig. 7 shows that the deeply oxidized domains expanded only from step edges. The image showed a mixture of $(3\times 5)$ domains $B$ and new domains $K$. Most of the surface area was recovered as $(3\times 5)$ domains after annealing at 900 K.

Further oxidation using 9-L $O_3$ on the surface at 600 K caused the deeply oxidized area to reach the opposite step edge. On this surface, "holes" were produced with an apparent depth of ~0.25 nm as shown in the cross-section $a1$–$a2$ in Fig. 8. This indicates a depth of a few layers. The cross-section $b1$–$b2$ indicates that the apparent corrugation of smaller holes is ~0.07 nm, and so the pseudo-$(2\sqrt{2}\times 2\sqrt{2})R45°$ nets, indicated at $c1$ for example, were produced on a three-layer thick film. When this surface was annealed at 900 K in vacuum, the LEED pattern was a mixture of the $(2\sqrt{2}\times 2\sqrt{2})R45°$ and $(3\times 5)$ structures.

Fig. 9(a) shows an STM image obtained after oxidation using 15-L $O_3$ on the surface at 600 K. Trigonal prism clusters were observed, and most

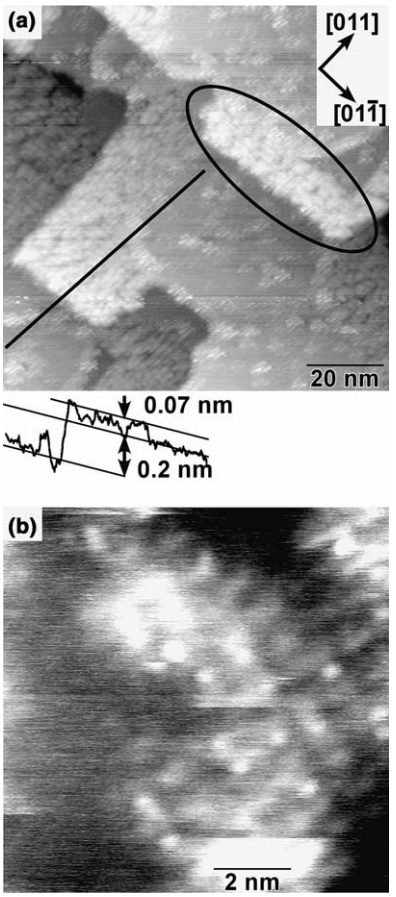


Fig. 6. STM topographs of the $(3\times 5)$ oxide film on Pt(100) after further oxidation using 3-L $O_3$ with the substrate at 300 K. (a) Oxidation occurs principally at step edges (as highlighted by the superimposed black ellipse) ($V_s = 0.47$ V, $I_t = 0.47$ nA). The cross-section of the line scan indicated in the image is shown directly below. (b) Expanded view of a deeply oxidized domain ($V_s = 1$ V, $I_t = 0.48$ nA).

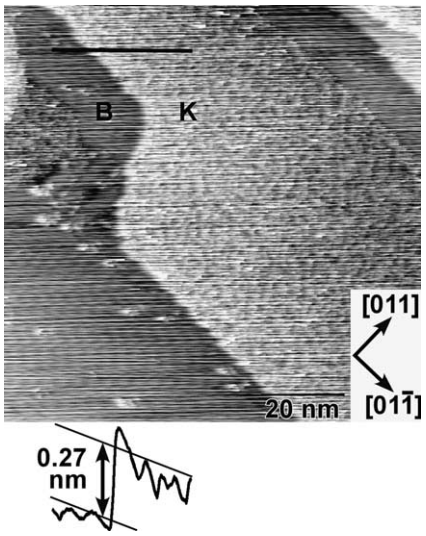


Fig. 7. STM topograph of the $(3\times5)$ oxide film on Pt(1 0 0) after further oxidation using 3-L $O_3$ with the substrate at 600 K ($V_s$ = 1 V, $I_t$ = 0.16 nA). Domains *B* and *K* are assigned to the $(3\times5)$ oxide film and more deeply oxidized regions, respectively. The cross-section of the line scan indicated in the image is shown directly below.

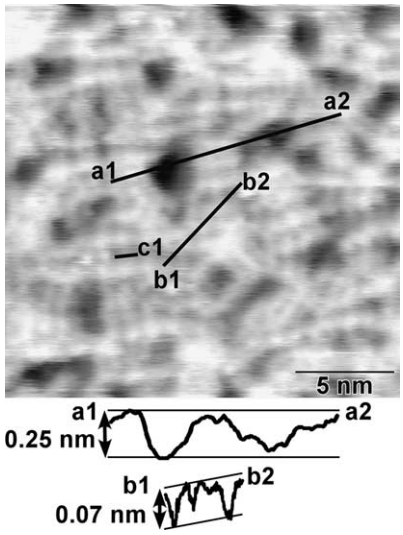


Fig. 8. STM topograph of the $(3\times5)$ oxide film on Pt(1 0 0) after further oxidation using 9-L $O_3$ with the substrate at 600 K ($V_s$ = 1.1 V, $I_t$ = 0.47 nA). Cross-sections along the lines *a*1–*a*2 and *b*1–*b*2 indicated in the image are shown directly below. A $(2\sqrt{2}\times2\sqrt{2})R45°$-like structure is observed (denoted as *c*1).

step edges of these clusters were along the [0 1 1] and equivalent directions. The area highlighted

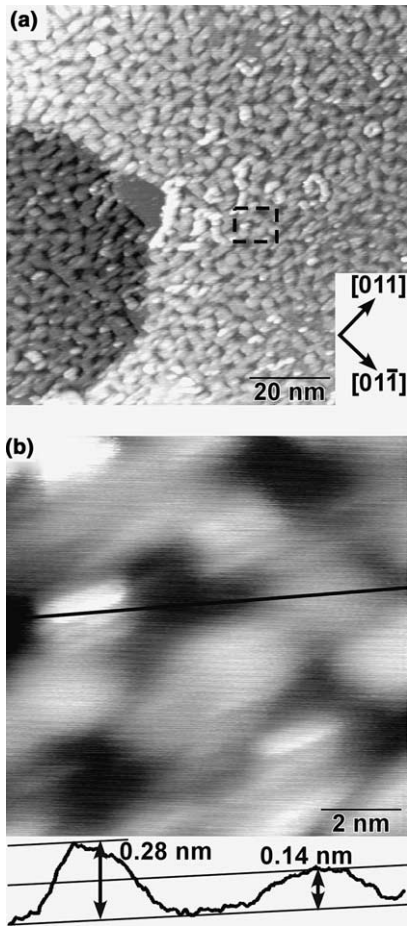


Fig. 9. STM topographs of the $(3\times5)$ oxide film on Pt(1 0 0) after further oxidation using 15-L $O_3$ with the substrate at 600 K. (a) Titania clusters ($V_s$ = 1.1 V, $I_t$ = 0.78 nA). (b) Expanded view of the region indicated by the superimposed dashed box in (a) ($V_s$ = 0.2 V, $I_t$ = 0.74 nA). The cross-section of the line scan indicated in the image is shown directly below.

by the superimposed black box in Fig. 9(a) is shown on an expanded scale in Fig. 9(b). The heights of the clusters are 0.14, 0.21 or 0.28 nm as the cross-section along the indicated black line shows. A mixture of $(4\times13)$, $(2\sqrt{2}\times2\sqrt{2})R45°$ and $(3\times5)$ domains and $TiO_2$ clusters were produced after annealing this surface in vacuum at 900 K.

Another set of experiments were carried out in which the Ti deposition on Pt(1 0 0) was performed in a partial pressure of $O_3$ (rather than $O_2$) with the substrate at 700–900 K. This procedure, or anneal-

ing the $(3 \times 5)$ film in $O_3$ to near 900 K gave LEED patterns corresponding to the $(4 \times 13)$ and "24-structure" [8] films. The best LEED patterns were obtained after annealing these films at the lowest temperature of 1000 K. While $(4 \times 13)$, $(2\sqrt{2} \times 2\sqrt{2})R45°$ and $(3 \times 5)$ domains and $TiO_2$ clusters were observed on these surfaces after annealing to 1000 K in vacuum, a "flat" oxide film was never observed.

### 3.2. NO adsorption and reduction via oxidation of a titanium oxide film on Pt(100)

A submonolayer, $(3 \times 5)$ oxide film on Pt(100) at 300–1000 K was not oxidized by 100-L $O_2$ exposure [8], presumably due to the low sticking probability on Pt(100) estimated at $\sim 10^{-3}$ [31]. Another potential oxidant, NO, was used to examine the stability of titanium oxide films on Pt(100) to oxidation reactions. NO TPD spectra were acquired following NO exposures on the $(5 \times 20)$-Pt(100) surface, a submonolayer $(3 \times 5)$ oxide film surface (Pt/Ti/O AES ratio of 1/1/1), and a several monolayer thick $(3 \times 5)$ oxide film surface (Pt/Ti/O AES ratio of 1/3.2/3.2). A 6-L NO exposure was given on each these surfaces at 200 K and then the TPD spectra were obtained. This entailed heating the surfaces to 800 K. On Pt(100), TPD peaks at 450–500 K were observed for signals at 28 ($N_2$), 30 (NO) and 44 ($N_2O$) amu, and at 700 K for 32 ($O_2$) amu. This behavior is similar to that described in a previous report [2]. The submonolayer $(3 \times 5)$ oxide film surface gave smaller TPD peaks for $N_2$, NO and $N_2O$, but no $O_2$ peak was detected. Also, an additional LEED pattern indicating a $(2\sqrt{2} \times 2\sqrt{2})R45°$ structure appeared after the TPD measurements. For the $(3 \times 5)$ oxide film that was several monolayer thick, no desorption peaks and no change in the LEED pattern were observed during or after TPD measurements.

### 3.3. CO adsorption on titanium oxide films on Pt(100)

CO adsorption on several substrates at 210 K was used to probe aspects of the surface chemistry of titanium oxide films on Pt(100). Fig. 10 shows CO TPD spectra following 6-L CO adsorption

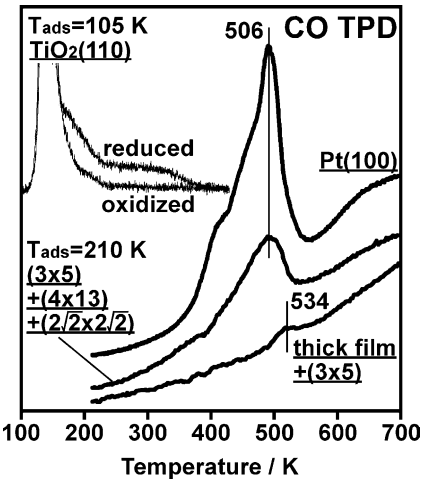


Fig. 10. CO TPD spectra after 6-L CO exposures on the clean $(5 \times 20)$-Pt(100) surface, a surface characterized by the presence of a mixture of $(3 \times 5)$, $(4 \times 13)$, $(2\sqrt{2} \times 2\sqrt{2})R45°$ oxide domains along with bare Pt(100), and thick titania films with $(3 \times 5)$ oxide domains on the Pt(100) surface. Exposures were carried out with the surfaces at 210 K. CO TPD spectra from $TiO_2$(110) [14] are reproduced as an inset in the upper left hand corner. No desorption peak at 44 amu ($CO_2$) was observed in these experiments.

on a (i) $(5 \times 20)$-Pt(100) surface, (ii) partially covered Pt(100) surface containing a mixture of $(3 \times 5)$, $(2\sqrt{2} \times 2\sqrt{2})R45°$, and $(4 \times 13)$ oxide domains and bare, Pt(100) domains, and (iii) thick titanium oxide film with $(3 \times 5)$ domains on Pt(100) (as shown in Fig. 12 of Ref. [8]). CO TPD spectra from oxidized and reduced $TiO_2$(110) surfaces are also displayed as a reference. CO TPD peaks were observed at 506 K from both clean Pt(100) and the partially oxide-covered Pt(100) surface. The Pt(100) results were similar to those in a previous study [24]. The mixture of oxide domains that partially covered the Pt(100) surface only served to reduce the CO TPD peak area, i.e., reduce the amount of adsorbed CO, from that on the oxide-free Pt(100) surface. Thick titanium oxide films essentially eliminated CO adsorption on the substrate surface at 210 K, but a small (~0.02 ML) TPD peak was seen at 534 K. Identical CO TPD spectra were obtained from a 2-ML thick $(3 \times 5)$ oxide film on Pt(100). No $CO_2$ TPD peak was observed from any of these surfaces after CO adsorption.

In addition, the $(2\sqrt{2}\times 2\sqrt{2})R45°$ domains on a partially covered Pt(100) surface containing a mixture of domains at 300 K were observed by STM in a flow of CO at $6.7\times 10^{-5}$ Pa. No changes in structure were observed. Also, the $(3\times 5)$ oxide film on Pt(100) was not reduced in a CO flow at $10^{-5}$ Pa with the substrate 750 K as checked by LEED and AES. Furthermore, no carbon was detected by AES after all of the experiments involving CO adsorption and TPD, which included heating to 700 K.

### 3.4. HCOOH adsorption and decomposition on titanium oxide films on Pt(100)

TPD spectra of HCOOH following adsorption of HCOOH on a $(5\times 20)$-Pt(100) surface and $(3\times 5)$ titanium oxide film on Pt(100) are shown in Fig. 11. A HCOOH TPD spectrum after HCOOH adsorption on a reduced $TiO_2$(001) surface that was produced by $Ar^+$-ion sputtering is also displayed [25]. In our experiments, a 30-L HCOOH exposure was made on the samples at 150 K, and then TPD curves were obtained during heating to 800 K. Signals in TPD were monitored at 46 (HCOOH), 2 ($H_2$), 18 ($H_2O$), 28 (CO), and 44 ($CO_2$) amu. TPD peaks appropriate for HCOOH desorption, including the cracking fractions at other masses, appeared at 189 and 330 K on Pt(100). The low- and high-temperature peaks are attributed to molecular desorption of HCOOH from the physisorbed multilayer and chemisorbed layer, respectively. No desorption of other decomposition products was observed, and no signals due to C or O on the surface were detected by AES after the TPD scan. Because HCOOH adsorption and desorption from Pt(100) has not been reported previously, we took extra care to insure that our TPD results reproducible, and the Pt(100) surface order and cleanliness were checked by AES, LEED and CO TPD before and after the HCOOH experiments.

The HCOOH TPD spectrum after HCOOH adsorption on a $(3\times 5)$ oxide film on Pt(100), which contained some $TiO_2$ clusters and 2% bare-Pt sites, gave two HCOOH desorption peaks at 189 and 371 K. These can be attributed to the same origins as above. No desorption of other

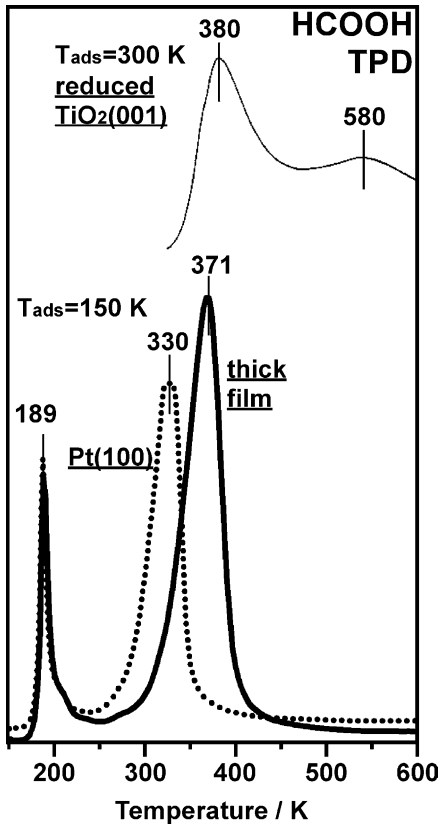


Fig. 11. HCOOH TPD spectra after 30-L HCOOH exposures on the clean $(5\times 20)$-Pt(100) surface and thick titania films with $(3\times 5)$ oxide domains on the Pt(100) surface. Exposures were carried out with the surfaces at 150 K. A HCOOH TPD spectrum from a reduced $TiO_2$(001) surface [25] is reproduced as an inset in the upper right hand corner. No desorption peaks at 2, 18, 28 and 44 amu were observed in these experiments other than the expected cracking fragments of HCOOH in the mass spectrometer.

decomposition products was observed, and the Pt:Ti:O AES ratio characterizing this surface was unchanged at 1:3:3 after the TPD scan.

HCOOH adsorption and desorption from a $(4\times 13)$ oxide film on Pt(100) was also examined by TPD during which the sample was heated to 800 K. No clear HCOOH (or other product) desorption peaks were observed during TPD, however, small, ambiguous desorption features for $H_2O$ and $CO_2$ were observed around 280–330 and 330 K, respectively. This indicates that the surface was nearly inert for HCOOH adsorption.

However, the LEED pattern changed to indicate a mixture of $(3\times5)$ and $(2\sqrt{2}\times2\sqrt{2})R45°$ domains after HCOOH exposure and heating in TPD, and the Pt/Ti/O AES ratio changed from 1:2.5:3.8 before HCOOH exposure to 1:2.5:2.8 after TPD.

### 3.5. $H_2$ exposures on titanium oxide films on Pt(100)

Adsorption of $H_2$ and possible reduction of a $(3\times5)$ oxide film on Pt(100), characterized by a Pt/Ti/O AES ratio of 1:3:3, was investigated. The $(3\times5)$ surface at 300 K was exposed to $1.3\times10^{-5}$ Pa $H_2$ and to a combined mixture of CO and $H_2$ gases, each at a partial pressure of $1.3\times10^{-5}$ Pa, with the sample at 300–750 K. During and subsequent to these experiments, no change was observed in the LEED patterns or AES spectra. These observations are consistent with previous results on $TiO_2$(110) surfaces indicating that either $H_2$ does not dissociatively adsorb at fully oxidized sites or $H_2$ rapidly dissociatively adsorbs and recombines at defect sites with O vacancies [15,16].

## 4. Discussion

In a previous paper [8], we characterized a monolayer titanium-oxide film exhibiting a $(3\times5)$ structure on Pt(100) as due to $Ti_2O_3$. Herein, we characterized changes that occur in this film during subsequent oxidation and reduction reactions. A variety of ordered-film structures were observed. A $(4\times13)$ structure was produced locally by $O_3$ or $NO_2$ oxidation of the $(3\times5)$-$Ti_2O_3$ film at 600 K and annealing at 700–950 K in vacuum. A $(2\sqrt{2}\times2\sqrt{2})R45°$ structure was formed locally by annealing of the $(4\times13)$ structure at 1000–1100 K in vacuum, and this structure decomposed to the $(3\times5)$ structure after annealing above 1200 K in vacuum. Also, the reactivity of these films depended on their structure. The $(3\times5)$ domains were oxidized with strong oxidizing agents, but inert against several reducing agents under UHV conditions. $O_3$ oxidation of the $(3\times5)$-$Ti_2O_3$ film at 600 K caused crystallization in the titanium oxide film. These crystals decomposed at 900 K and agglomerated to form $TiO_2$ clusters and $(4\times13)$, $(2\sqrt{2}\times2\times2)R45°$, and $(3\times5)$ structures. NO was reduced on the $(3\times5)$-$Ti_2O_3$ film because of NO decomposition at Pt sites and this oxidized the $(3\times5)$ film surface to form the $(2\sqrt{2}\times2\sqrt{2})R45°$ structure. HCOOH adsorbed reversibly on $(3\times5)$ terraces, but the $(4\times13)$ domains were reduced by HCOOH to form $(3\times5)$ and $(2\sqrt{2}\times2\sqrt{2})R45°$ domains. No reduction with $H_2$ was observed on the $(3\times5)$ domains, and titanium oxide films blocked CO adsorption sites above 210 K.

It is imperative to determine the atomic composition and structure of these titanium oxide films if we are to develop structure-property relationships and better understand the origin of their chemical properties. Theoretical calculations, along with additional experimental studies, are critically needed to properly elucidate these oxide structures. However, it is useful to propose at this time tentative models for the two new, ordered, titanium-oxide film structures on Pt(100) in hopes of stimulating such calculations and further experiments.

### 4.1. Proposed model of a titanium oxide film on Pt(100) with a $(4\times13)$ structure

Fig. 12(a) provides a high-resolution STM image of a titanium oxide film on Pt(100) with a $(4\times13)$ structure. Two domains can be observed in Fig. 12(a), one showing bright dots along the $y1$–$y3$ rows and the other showing bright dots along the $y4$–$y5$ rows. The Moiré pattern can be explained by a mismatch between the –Ti–O– nets in the oxide film and the Pt(100) substrate. Very bright spots might originate from Ti atoms "lifted up" on top of Pt atoms such as that which occurs at a crossing of $x1$ and $y1$.

A schematic drawing of our proposed model for this oxide structure is given in Fig. 12(b). The superimposed white rectangles indicate the unit cell of the $(4\times13)$ structure. The smaller, "square-net" sub-structures have atomic positions for Ti and O that are similar to the superimposed first and second layers of the $TiO_2$(001)

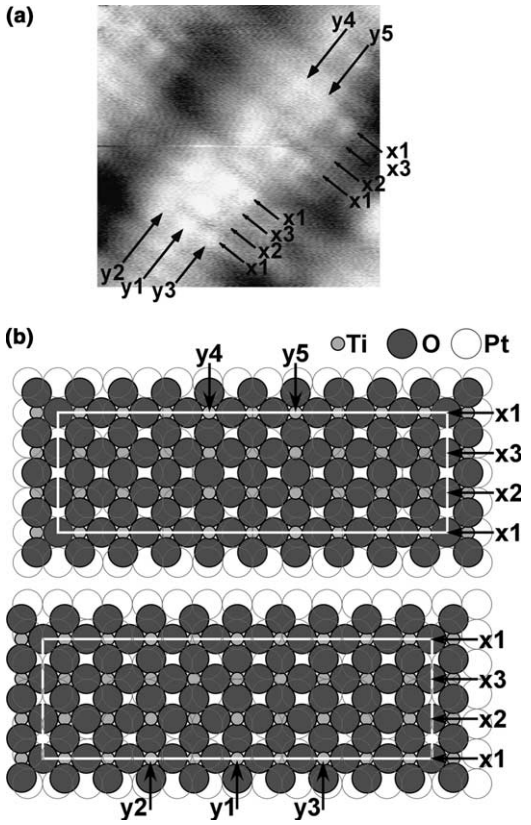


Fig. 12. (a) STM topograph from a titanium-oxide film on Pt(100) exhibiting a $(4 \times 13)$ structure. (b) Tentative model of the $(4 \times 13)$ structure. The superimposed white rectangle indicates the $(4 \times 13)$ unit cell. The rows $x1$–5 and $y1$–3 correspond to each other in each figure.

surface [26]. A similar, square structure was also observed on a $SrTiO_3(001)$ surface [27]. The numbers of Ti and O atoms in a $(1 \times 1)$ unit cell within this model are $27/52 = 0.52$ and $54/52 = 1.04$, respectively. The Ti density was measured to be almost the same as that for the $(3 \times 5)$ film [8], and the model is consistent with XPS spectra which indicate that the composition in this film corresponds to $TiO_2$ [8]. Thus, the titanium oxide film on Pt(100) with a $(4 \times 13)$ structure consists of one layer of a $TiO_2$ film. It is possible that screening effects by the Pt substrate cause the observed lower binding energies of the Ti 2*p* and O 1*s* peaks in XPS from this monolayer film compared to those of two-layer $TiO_x$ films on Pt(100) [8,28].

### *4.2. Proposed model of a titanium oxide film on Pt(100) with a $(2\sqrt{2} \times 2\sqrt{2})R45°$ structure*

A high-resolution STM image of a titanium oxide film on Pt(100) with a $(2\sqrt{2} \times 2\sqrt{2})R45°$ structure is given in Fig. 13(a). Our proposed model for this oxide structure is provided schematically in Fig. 13(b). This structure consists of one on-top Ti atom (*T*1), four Ti atoms near four-fold-substrate sites (*T*2), four O atoms near four-fold-substrate sites (*O*1), and four O atoms near two-fold-substrate bridge sites (*O*2). The brightest spots in STM topographs are assigned to *T*1, and the two *T*2 atoms appear to be observed as bright lines. The darkest spots are assigned to the Pt substrate because the apparent corrugation of 0.07 nm

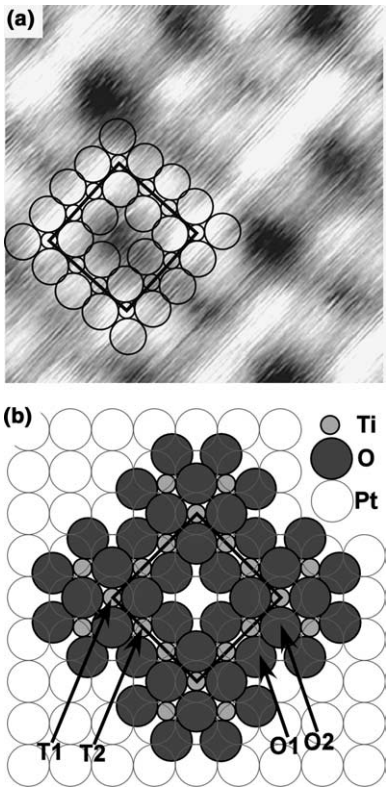


Fig. 13. (a) STM topograph from a titanium-oxide film on Pt(100) exhibiting a $(2\sqrt{2} \times 2\sqrt{2})R45°$ structure. (b) Tentative model of the $(2\sqrt{2} \times 2\sqrt{2})R45°$ structure. The superimposed black squares indicate the $(2\sqrt{2} \times 2\sqrt{2})R45°$ unit cell. This structure presents two different environments for Ti atoms (*T*1 and *T*2) and O atoms (*O*1 and *O*2).

is close to the 0.06–0.07-nm apparent thickness of single layers of oxide in the $(3\times5)$-$Ti_2O_3$ film or $TiO_2$ islands (see Fig. 9 in this report and Figs. 5 and 9 of Ref. [8]). This structure can be explained as arising from a crossing of short, $TiO_2$ rows which creates a local structure reminiscent of the 5-fold Ti atoms and their neighboring O atoms on the $TiO_2(1\,1\,0)$ surface [10]. One Ti and four O atoms are shared by two crossing rows. The densities of Ti and O atoms in a $(1\times1)$ unit cell in this model are 5/8 = 0.625 and 8/8 = 1, respectively. This Ti density is higher than those for the $(3\times5)$ and $(4\times13)$ structures and lower than that for the "24-structure" [8]. The ideal composition within this model is $Ti_5O_8$, which is consistent with the range of $TiO_{2-1.5}$ indicated by XPS spectra [8]. A lower binding energy than expected in XPS was observed for Ti 2*p* peaks corresponding to $Ti^{4+}$ and $Ti^{3+}$ states and O 1*s* peaks from this one-layer thick oxide structure and this can be explained in the same manner as above for the $(4\times13)$ oxide film [28].

Submonolayer coverages of $(2\sqrt{2}\times2\sqrt{2})R45°$ oxide films were transformed to $(3\times5)$ structures by annealing at 1200 K in vacuum, while the complete $(2\sqrt{2}\times2\sqrt{2})R45°$-$Ti_5O_8$ film was produced by decomposition of thick titanium-oxide films at 1300 K in vacuum [8]. This indicates that the $(2\sqrt{2}\times2\sqrt{2})R45°$ structure was formed below 1200 K by agglomeration of diffusing Ti and O atoms created by the decomposition of $TiO_2$ clusters. The $(4\times13)$-$TiO_2$ structure could not be produced by high-temperature annealing of thick titanium-oxide films. This result is consistent with our proposal that the $(2\sqrt{2}\times2\sqrt{2})R45°$-$Ti_5O_8$ film is less oxidized than the $(4\times13)$-$TiO_2$ film.

It is interesting to note that, as shown within the circle of Fig. 4(b) and in Fig. 5, the *H*1 defects are considered to be due to population of a second layer, the *H*2 defects might arise from Ti atoms sitting in the center holes of the unit cells, and the *H*3 defects are due to a rotation of the titanium oxide net away from the normal structure by 45 degrees. Intentional population and control of these defects might enable us to control chemical reactivity at the surface or physical properties such as those required for developing nano-sized data storage applications.

### *4.3. Reactions in deep oxidation of titanium oxide films on Pt(1 0 0) by using $O_3$ and $NO_2$*

Bright spots in the image shown in Fig. 6(b) following deep oxidation of the $(3\times5)$-$Ti_2O_3$ film on Pt(1 0 0), i.e., after 3-L $O_3$ oxidation at 300 K, might be due to Ti atoms "lifted up" by incorporation of additional oxygen into the subsurface region of the oxide film as the film thickens. The STM image in Fig. 8, obtained after deep oxidation by a 9-L $O_3$ exposure on the substrate at 600 K, also suggests that Ti atoms were lifted up by a thickening of the oxide to form a film consisting of 2–3 oxide layers. An oxidation mechanism consistent with these STM images is one in which Ti atoms in the bottom oxide layer (in contact with the Pt substrate) diffuse to the surface of the oxide film. Additional oxygen is incorporated into the bottom oxide layer to fully oxidize the remaining Ti atoms present and into the top oxide layer to oxidize the diffused Ti atoms. This leads to a thickening of the oxide film. Further oxidation at defect sites like step edges or domain boundaries of the initial $(3\times5)$-$Ti_2O_3$ film is preferred over oxidation in the middle of terraces. Within this mechanism, heating the film to 600 K enhanced Ti diffusion to the film surface and deeper oxidation.

In the final stage of deep oxidation, as shown in Fig. 9, oxide prism-islands or crystals with a thickness of 2–4 layers were formed. This was deduced from the apparent corrugation in the STM images and the 0.07-nm thickness of each $TiO_2$ layer in the film. These prism-islands disappeared after annealing at 1000 K, and thus were less stable than those observed after annealing thicker oxide films that exceeded monolayer coverage at 1000 K. Most prism-islands or crystals produced by deep oxidation decomposed at 900 K to form $(4\times13)$, $(2\sqrt{2}\times2\sqrt{2})R45°$, and $(3\times5)$ structures and larger $TiO_2$ clusters. While it is clear that using the stronger oxidants $O_3$ and $NO_2$, compared to $O_2$, can provide different synthetic strategies for new, titanium-oxide film structures on Pt(1 0 0), selectivity for the formation of a single, oxide-film structure is low under all of these conditions. Control of the film structure is difficult because processing inhomogeneous multilayer films causes

decomposition and/or reconstruction to competitively form new compositions and structures.

### 4.4. NO reduction at titanium oxide films on Pt(100)

Decomposition of NO on a Pt(100) surface leads to the formation of 0.4-ML O adatoms and subsequent $O_2$ desorption in TPD after NO adsorption at 200 K [29,30]. Even though NO adsorption and reduction occurs on submonolayer $(3\times5)$-$Ti_2O_3$ films on Pt(100), no $O_2$ desorption was observed following NO exposures on these surfaces. This indicates that all of the O adatoms produced by NO decomposition at Pt sites were consumed by oxidation of the $(3\times5)$ structure to form the $(2\sqrt{2}\times2\sqrt{2})R45°$ structure.

No NO desorption was observed in TPD following NO exposures on thick titanium oxide films with coverages of several monolayers on Pt(100). This confirms that NO is strongly adsorbed and decomposes, not on the $(3\times5)$-$Ti_2O_3$ or $TiO_2$ islands, but only at Pt sites to oxidize the $(3\times5)$-$Ti_2O_3$ domains. This is different behavior from that attributed to $Ti^{3+}$ sites on $TiO_2$(110) [19].

### 4.5. Adsorption of CO on titanium oxide films on Pt(100)

The presence of the $(3\times5)$-$Ti_2O_3$ film on Pt(100) blocked all adsorption of CO above 230 K. This is consistent with reports on encapsulated Pt clusters [11,32]. The small CO TPD peak observed from the $(3\times5)$ film surface is presumably due to irregular Pt-sites (as seen in Fig. 12(c) or (d) of Ref. [8]). The area of available, bare-Pt sites on the $(3\times5)$-$Ti_2O_3$ film on Pt(100) surface that we investigated was estimated to be about 2% by using the CO TPD peak areas from the clean and oxide-covered Pt(100) surface. A CO TPD peak near 376 K that has been attributed to $Pt_3$ Ti alloy sites [33] was not found from the oxide-covered Pt(100) surface. Thus, CO TPD confirms no formation of a $Pt_3$ Ti surface alloy during preparation of these oxide-covered Pt(100) surfaces, which is consistent with STM and XPD results [8].

No chemical reaction of CO with deeply oxidized titanium-oxide films on Pt(100) was observed under the conditions of this study, and in particular, such surfaces did not oxidize adsorbed CO to $CO_2$ during TPD.

### 4.6. Adsorption and reaction of HCOOH on Pt(100) and titanium oxide films on Pt(100)

Surface-bound formate (HCOO) species produced by dissociative adsorption of formic acid have been studied as important intermediates in the water-gas shift and methanol synthesis reactions [2,34] on many metal single-crystal surfaces. Reactions of formic acid on metal surfaces are grouped into four types: type I—dehydrogenation; type II—dehydrogenation and dehydration; type III—dehydrogenation, dehydration and complete decomposition; and type IV—desorption as formic acid without dissociative adsorption below 200 K. Reactions of formic acid on Pt surfaces are expected to depend on the surface structure, but no information until now has been reported on Pt(100) (Table 1).

Molecular desorption of formic acid has never been observed on metal surfaces above 300 K,

Table 1
Reactions of formic acid on metal surfaces

| Type | Reaction | Surface |
|---|---|---|
| I | $HCOOH_{ad} \rightarrow HCOO_{ad} + H_{ad}$ $\rightarrow CO_2 + H_2$ | Pt(111) [35], Cu(110) [36], Cu(100) [37], Ag(111) [38] |
| II | $HCOOH_{ad} \rightarrow HCOO_{ad} + H_{ad}$ $\rightarrow CO_2 + H_2 + CO + H_2O$ | Ni(110) [39], Ni(100) [40], Ni(111) [41], Fe(100) [42], Ru(100) [43], Au(110) [44], Pd(100) [45], Pd(110) [46] |
| III | $HCOOH_{ad} \rightarrow HCOO_{ad} + H_{ad}$ $\rightarrow CO_2 + H_2 + CO + H_2O + C_{ad} + O_{ad}$ | W(100) [47], Al(111) [48], Mo(100) [49] |
| IV | $HCOOH_{ad} \rightarrow HCOOH$ | Pt(110) [50], Au(111) [51], Cu(111) [52] |
| V | $HCOOH_{ad} \rightarrow HCOO_{ad} + H_{ad} \rightarrow HCOOH$ | Pt(100) [This work] |

but it has been reported from a NiO(1 0 0)/Mo(1 1 0) surface at 375 K [53]. The formic acid reaction mechanism on Pt(1 0 0) might be as explained below by analogy. However, additional spectroscopic information is certainly needed to confirm this proposal. According to our model, molecularly adsorbed formic acid desorbs at 189 K and dissociatively chemisorbed formic acid undergoes recombinative desorption at 330 K:

$$HCOOH_{ad} \rightarrow HCOOH \quad (189\ K) \tag{1}$$

$$HCOOH_{ad} \rightarrow HCOO_{ad} + H_{ad} \quad (< 200\ K) \tag{2}$$

$$HCOO_{ad} + H_{ad} \rightarrow HCOOH \quad (330\ K) \tag{3}$$

From the $(3\times5)$-$Ti_2O_3$ film on Pt(1 0 0), the HCOOH TPD peak at 371 K could arise from the recombination of surface-bound formate and hydroxyl groups as detailed below:

$$HCOOH_{ad} \rightarrow HCOOH \quad (189\ K) \tag{4}$$

$$HCOOH_{ad} + O_{lattice} \rightarrow HCOO_{ad} + H - O_{lattice} \quad (< 200\ K) \tag{5}$$

$$HCOO_{ad} + H - O_{lattice} \rightarrow HCOOH + O_{lattice} \quad (371\ K) \tag{6}$$

The same reaction was observed in the $(2\times1)$-formate adlayer on the rutile-$TiO_2$(1 1 0) surface around 350 K [12] and on a reduced $TiO_2$(0 0 1) surface [25]. $H_2$ desorption at 400 K or decomposition of formate to $H_2$, $H_2O$, CO and $CO_2$ around 570 K [12] or to formaldehyde around 540 K was not observed [25]. Formate and hydrogen did not recombine substantially at bare-Pt sites at 330 K. The HCOOH TPD peak area at 371 K observed from the $(3\times5)$-$Ti_2O_3$ film on Pt(1 0 0) was close to that from the Pt(1 0 0) surface at 330 K, which indicates that formic acid was adsorbed at a similar coverage on both surfaces.

The $(4\times13)$ oxide domains on Pt(1 0 0) might be reduced in the following manner, as was suggested on $TiO_2$(1 1 0) [12]:

$$HCOOH_{ad} + O_{lattice} \rightarrow HCOO_{ad} + H - O_{lattice} \quad (< 200\ K) \tag{7}$$

$$2H - O_{lattice} \rightarrow O_{lattice} + H_2O \quad (280\ K) \tag{8}$$

$$2HCOO_{ad} + O_{lattice} \rightarrow H_2O + 2CO_2 \quad (330\ K) \tag{9}$$

## 5. Conclusions

Fundamental studies of titanium oxide-Pt(1 0 0) interfaces were carried out in which we placed special emphasis on the influence of oxidation and reduction reactions on the surface structure of $TiO_x$ films on Pt(1 0 0). In a previous paper [8], we showed that a titanium-oxide monolayer film exhibiting a $(3\times5)$ structure, attributed to $Ti_2O_3$, can be produced by Ti evaporation in an $O_2$ background on Pt(1 0 0) and annealing in $O_2$. Herein, we investigated the microscopic structure and chemical properties of more deeply oxidized films on Pt(1 0 0).

A $(4\times13)$-$TiO_2$ film can be produced locally by further oxidation, using $O_3$ or $NO_2$, of the $(3\times5)$-$Ti_2O_3$ surface at 600 K and annealing at 700–950 K in vacuum. A tentative model of this structure is proposed in which a one-layer oxide film is formed with square –Ti–O– ''nets'', similar in structure to the superposition of the first and second layers of the $TiO_2$(0 0 1) surface. This oxide film covers the Pt(1 0 0) substrate to produce a Moiré pattern due to the incommensurate structures.

A $(2\sqrt{2}\times2\sqrt{2})R45°$-$Ti_5O_8$ film structure can also be formed locally by annealing the $(4\times3)$-$TiO_2$ film on Pt(1 0 0) at 1000–1100 K in vacuum. A tentative model of this structure is also proposed, and this involves ''crossings'' of short $TiO_2$ rows. Three distinct types of defect sites in this film were identified. This oxide film structure decomposed to the $(3\times5)$ structure by annealing above 1200 K in vacuum.

Deeper oxidation, using $O_3$, of the $(3\times5)$ film at 600 K caused crystallization of the titanium oxide film. These prism-islands or crystals decomposed at 900 K to form $(4\times13)$, $(2\sqrt{2}\times2\sqrt{2})R45°$ and $(3\times5)$ structures and larger $TiO_2$ clusters.

Thus, the $(3\times5)$-$Ti_2O_3$ domains on Pt(1 0 0) can be oxidized further by using strong oxidizing agents. But the $(3\times5)$-$Ti_2O_3$ domains are inert to reducing agents under our conditions. NO exposures on a $(3\times5)$-$Ti_2O_3$ film on Pt(1 0 0) led to NO reduction via NO decomposition at Pt sites and oxidation of

the $(3\times5)$-$Ti_2O_3$ structure to form the $(2\sqrt{2}\times 2\sqrt{2})R45^\circ$ structure. Titanium oxide films on Pt(100) blocked CO adsorption above 210 K. No reduction of the $(3\times5)$ domains was observed by any exposures to $H_2$ or $CO+H_2$ mixtures.

Additionally, reduction involving formic acid (HCOOH) was investigated. Because it has not been discussed previously, we also report that HCOOH adsorbs reversibly on clean Pt(100) surfaces and desorbs in TPD at 189 at 330 K. These two peaks are assigned to desorption of molecularly adsorbed formic acid and recombinative desorption of dissociatively chemisorbed formic acid, respectively. From $(3\times5)$-$Ti_2O_3$ terraces, low-temperature molecular desorption of HCOOH was observed and no reduction of the $(3\times5)$-$Ti_2O_3$ domains occurred. On the other hand, $(4\times13)$ oxide domains were reduced by reaction with HCOOH to form $(3\times5)$ and $(2\sqrt{2}\times2\sqrt{2})R45^\circ$ domains on the Pt(100) surface.

We suggest that these results for oxidation and reduction reactions on the surface structure of $TiO_x$ films on Pt(100) have important consequences for the understanding and modeling of catalysis of related systems. While theoretical calculations are critically needed to properly elucidate these oxide structures, tentative "net-like" models for two new, ordered, titanium-oxide film structures on Pt(100) are proposed in hopes of stimulating such calculations and further experiments. These particular oxide net structures have an additional significance in their subsequent use as masks or templates on Pt(100) in studies relevant to nanotechnology.

## Acknowledgment

This work was partially supported by the Analytical and Surface Chemistry Program in the Division of Chemistry, National Science Foundation.

## References

[1] S.A. Chambers, Surf. Sci. Rep. 39 (2000) 105.
[2] H. Nishimura, T. Yatsu, T. Fujitani, T. Uchijima, J. Nakamura, J. Mol. Catal. A 155 (2000) 3, and references therein.
[3] D. Hartmann, H. Knözinger, Z. für Physik Chem. 197 (1996) 113.
[4] C. Hardacre, G.M. Roe, R.M. Lambert, Surf. Sci. 326 (1995) 1.
[5] C. Xu, D.W.J. Goodman, Chem. Soc. Faraday Trans. 91 (1995) 3709.
[6] S. Surnev, L. Vitali, M.G. Ramsey, F.P. Netzer, G. Kresse, J. Hafner, Phys. Rev. B 61 (2000) 13945.
[7] U. Heiz, W. Schneider, in: K.H. Meiwes-Broer (Ed.), Metal Clusters at Surfaces, Springer-Verlag, Berlin, 2000, p. 243.
[8] T. Matsumoto, M. Batzill, S. Hsieh, B.E. Koel, Surf. Sci. (2004), in press. doi:10.1016/j.susc.2004.08.006.
[9] A.B. Boffa, H.C. Galloway, P.W. Jacobs, J.J. Benitez, J.T. Batteas, M. Salmeron, A.T. Bell, G.A. Somorjai, Surf. Sci. 326 (1995) 80, and references therein.
[10] H. Ohnishi, Y. Iwasawa, Phys. Rev. Lett. 76 (1996) 791.
[11] J.M. Herrman, M. Gravelle-Rumeau-Maillot, P.C. Gravelle, J. Catal. 104 (1987) 136.
[12] H. Ohnishi, T. Aruga, Y. Iwasawa, J. Catal. 146 (1994) 557.
[13] M.A. Henderson, S. Otero-Tapia, M.E. Castro, Faraday Discuss. 114 (1999) 313.
[14] A. Linsebigler, G. Lu, J.T. Yates Jr., J. Chem. Phys. 103 (1995) 9438.
[15] W. Göpel, G. Rocker, R. Feierabend, Phys. Rev. B 28 (1983) 3427.
[16] J. Leconte, A. Markovits, M.K. Skalli, C. Monot, A. Belmajdoub, Surf. Sci. 497 (2002) 194, and references therein.
[17] M.A. Henderson, Langmuir 12 (1996) 5093.
[18] M.B. Hugenschmidt, L. Gamble, C.T. Campbell, Surf. Sci. 302 (1994) 329.
[19] G. Lu, A. Linsebigler, J.T. Yates Jr., J. Phys. Chem. 98 (1994) 11733.
[20] M.A. Henderson, W.S. Epling, C.L. Perkins, C.H.F. Peden, U. Diebold, J. Phys. Chem. B 103 (1999) 5328.
[21] D. Beck, M. Batzill, C. Baur, K. Jooho, B.E. Koel, Rev. Sci. Instrum. 73 (2002) 1267.
[22] N. Saliba, D.H. Parker, B.E. Koel, Surf. Sci. 410 (1998) 270.
[23] L.E. Davis, N.C. McDonald, P.W. Palmberg, G.E. Riach, R.E. Weber, Handbook of Auger Electron Spectroscopy, Physical Electronics Industries Inc., Minnesota, 1976.
[24] M.A. Barteau, E.I. Ko, R.J. Madix, Surf. Sci. 102 (1981) 99.
[25] H. Idriss, V.S. Lusvardi, M.A. Barteau, Surf. Sci. 348 (1996) 39.
[26] V.E. Henrich, P.A. Cox, The Surface Science of Metal Oxides, Cambridge University Press, Cambridge, 1996.
[27] M.R. Castell, Surf. Sci. 505 (2002) 1.
[28] Y. Wu, E. Garfunkel, T.E. Madey, Surf. Sci. 365 (1996) 337.
[29] E.D.L. Rienks, J.W. Bakker, A. Baraldi, S.A.C. Carabineiro, S. Lizzit, C.J. Weststrate, B.E. Nieuwenhuys, Surf. Sci. 505 (2002) 1.
[30] J.M. Gohndrone, R.I. Masel, Surf. Sci. 209 (1989) 44.

[31] P.R. Norton, K. Griffiths, P.E. Binder, Surf. Sci. 138 (1984) 125.
[32] O. Dulub, W. Hebenstreit, U. Diebold, Phys. Rev. Lett. 84 (2000) 3646.
[33] S. Hsieh, T. Matsumoto, M. Batzill, C. Ho, B.E. Koel, in preparation.
[34] J.A. Rodriguez, D.W. Goodman, Surf. Sci. Rep. 14 (1991) 94, and references therein.
[35] M.A. Columbia, P.A. Thiel, Surf. Sci. 235 (1990) 53.
[36] R.J. Madix, S.G. Telford, Surf. Sci. 277 (1992) 246.
[37] L.H. Dubois, T.H. Ellis, B.R. Zegarski, S.D. Kevan, Surf. Sci. 172 (1986) 385.
[38] W.S. Sim, P. Gardner, D.A. King, J. Phys. Chem. 100 (1996) 12509.
[39] A. Yamakata, J. Kubota, J.N. Kondo, C. Hirose, K. Domen, F. Wakabayashi, J. Phys. Chem. B 107 (1997) 5177.
[40] J.B. Benziger, R.J. Madix, Surf. Sci. 79 (1979) 394.
[41] J.B. Benziger, G.R. Schoofs, J. Phys. Chem. 88 (1984) 4439.
[42] J.B. Benziger, R.J. Madix, J. Catal. 65 (1980) 49.
[43] L.A. Larson, J.T. Dickenson, Surf. Sci. 84 (1979) 17.
[44] M. Chtaib, P.A. Thiry, J.P. Delrue, J.J. Pireaux, R. Caudano, J. Electron Spectrosc. Relat. Phenom. 29 (1983) 293.
[45] D. Sander, W. Erley, J. Vac. Sci. Technol. A 8 (1990) 3357.
[46] N. Aas, L. Yongxue, M. Bowker, J. Phys. Condens. Matt. 3 (1991) 5281.
[47] A.K. Bhattacharya, Surf. Sci. 79 (1979) L341.
[48] P.R. Davies, M.W. Roberts, N. Shukla, J. Phys. Condens. Matt. 3 (1991) S237.
[49] S.L. Miles, S.L. Bernasek, J.L. Gland, Surf. Sci. 127 (1983) 271.
[50] T. Ohtani, J. Kubota, A. Wada, J.N. Kondo, K. Domen, C. Hirose, Surf. Sci. 368 (1996) 270.
[51] D.A. Outka, R.J. Madix, Surf. Sci. 179 (1987) 361.
[52] T. Matsumoto, R. Bennett, P. Stone, T. Yamada, K. Domen, M. Bowker, in press.
[53] C.M. Truong, M. Wu, D.W. Goodman, J. Chem. Phys. 97 (1992) 9447.